JOURNAL OF SOLID STATE CHEMISTRY 3, 411–419 (1971)

Structural and Phase Relationships among Trivalent Tungstates and Molybdates

K. NASSAU, J. W. SHIEVER, AND E. T. KEVE*

Bell Telephone Laboratories, Incorporated,
Murray Hill, New Jersey

Received January 6, 1971

Trivalent tungstates and molybdates of the type $L_2(MO_4)_3$ have been further investigated and a number of new phases are reported. Tungstate–molybdate phase diagrams for La, Sm, Gd, Ho, and In, including lattice parameters of the pseudoscheelite subcells where applicable, were studied and gave insight into structural relationships. It was found that the more than eight structures occurring can be organized into three families of structures.

A. Introduction

The trivalent metal tungstates and molybdates include a number of materials with interesting fluorescent, laser, piezoelectric, ferroelectric, and ferroelastic properties. They also provide a series of systems for crystallochemical and structural investigation. Previous reports of our work (*1*, *2*) have described the occurrence of at least six distinct structures among compounds of the type $L_2(MO_4)_3$ where L is a rare earth (or other trivalent element yielding identical or closely related structures) and M is W or Mo. Four of these structures have now been accurately determined, three (*3–5*) using crystals prepared during the course of this work.

Insight may be obtained on the relationships among these structures by the study of pseudobinary phase diagrams such as that of $Nd_2(WO_4)_3$–$Nd_2(MoO_4)_3$ system (*2*). In the present work, five additional tungstate–molybdate phase diagrams have been determined. A high-temperature phase transition previously unrecognized has been observed in $Gd_2(MoO_4)_3$ and several adjacent compounds. Compounds prepared by low-temperature sintering also revealed additional low-temperature phase transitions for Tb, Dy, Ho, and Y molybdates and Ho and Y tungstates. The surprisingly numerous types of structures present are now recognized to fall into three main groups, with variations being due to disordering and relatively small distortions in structures based on scheelite-type subcells.

* Present address: Mullard Research Laboratories, Redhill, Surrey, England.

Experimental procedures are the same as those described previously (*1*, *2*); references to earlier work of others will also be found there. Rode *et al.* (*6*) have also studied the lanthanide molybdates, confirming our work except for noting that those lanthanide molybdates reported by us to have the same structure as $Sc_2(WO_4)_3$, C, appeared to be slightly different on the basis of X-ray powder-diffraction patterns and were designated by them as C′.

B. Occurrence of Structures

The existence regions of the various types of structures are shown in Figs. 1 and 2 for molybdates and tungstates respectively; only those non-lanthanide compounds are included which have the same or closely related structures. These diagrams are based primarily on differential thermal analysis (DTA) data supported by quenching and X-ray diffraction work. Data differing significantly from that previously reported (*1*) is given in Table I. Also included are the data on the promethium compounds as reported by Weigel and Scherer (*7*); high-temperature transitions were not investigated in their work.

It is convenient to use three types of designations for these structures. In comparing the structures of different compounds, such as those of Figs. 1 and 2, the alphabetic designations "A", "C", etc., are convenient as a quick identification label. Since in most cases these identifications are made only from X-ray powder-diffraction data (Debye–Scherrer or

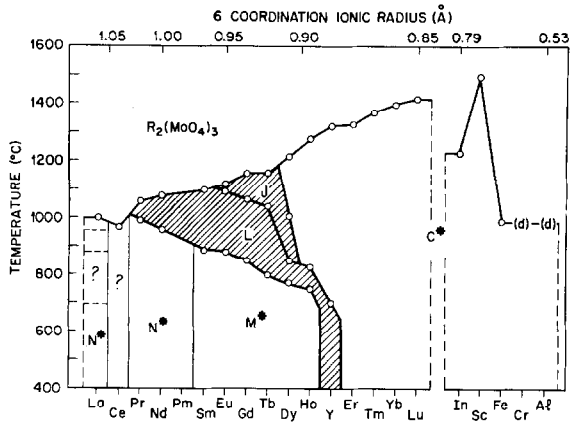

FIG. 1. Melting and transition temperatures and structure types occurring among $R_2(MoO_4)_3$ compounds.

Guinier photographs or diffractometer traces), subtle differences, e.g., slightly differing weak superlattice lines, must sometimes be ignored so that those designations shown with an asterisk such as "N*" and "C*" refer to a group of closely related, but not identical structures as discussed in Section E. When considering individual compounds, e.g. in the end-members of the phase diagrams of Section C, it is customary to use the prefixes α-, β-, etc. for the phases occurring with increasing temperatures. Finally, for discussion of an individual structure, the designation is customarily by the specific compound for which the structure was first solved. Thus one may speak of α-$Nd_2(WO_4)_3$ being part of the "A" field and having the α-$Eu_2(WO_4)_3$ structure. All three designations can be correlated from Figs. 1 and 2. Individual structures are further discussed in detail in Section E.

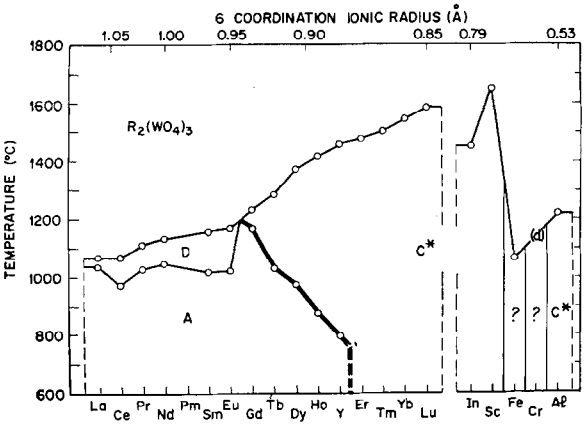

FIG. 2. Melting and transition temperatures and structure types occurring among $R_2(WO_4)_3$ compounds.

TABLE I

ADDITIONAL DTA DATA[a]

Compound	Transitions (°C) and phases	Melting point (°C)
$Pm_2(MoO_4)_3$	(N)	—
$Eu_2(MoO_4)_3$	(M) 880(L) ~ 1090 (J)	1120
$Gd_2(MoO_4)_3$	(M) 850(L) ~ 1070 (J)	1160
$Tb_2(MoO_4)_3$	(M) 800(L) ~ 1040 (J)	1160
$Dy_2(MoO_4)_3$	(M) 770(L)850(J)1010(C)	1220
$Ho_2(MoO_4)_3$	(M) 750(L)830(C)	1280
$Y_2(MoO_4)_3$	(L)700(C)	1325
$Pm_2(WO_4)_3$	(A)	—
$Ho_2(WO_4)_3$	(A) 875(C)	1415
$Y_2(WO_4)_3$	(A) 795(C)	1470

[a] Only data for compounds differing significantly from those of Ref. (*1*) are listed. Promethium data from Ref. (*3*).

The extra low-temperature phases and transitions for Tb, Dy, Ho, and Y molybdates and Ho and Y tungstates were obtained by sintering at 600°C; previously sintering had been performed at 700 to 1100°C (*1*). The $Ho_2(WO_4)_3$ transition is the only one which had been previously reported by others (at 935°C by Plyuschev and Amosov (*8*)). Complete conversion was not obtained in $Y_2(WO_4)_3$ even in 3 weeks. In the case of the Er, Tm, and Yb tungstates even 5 weeks sintering gave only very weak A-type diffraction lines and barely detectable A to C transitions in DTA at about 750°C; these data are not shown in Fig. 2 and Table I since there is some uncertainty. It is of course possible that similar low-temperature transitions also may occur in $Lu_2(WO_4)_3$, $Er_2(MoO_4)_3$, etc., at low temperatures but this was not further investigated since reaction is so slow that sintering is not a practicable technique.

C. Terbium, Gadolinium, and Related Molybdates

The β forms of $Tb_2(MoO_4)_3$ and $Gd_2(MoO_4)_3$ (and adjacent isostructural compounds) are particularly interesting in that their ferroelectric and ferroelastic properties are completely coupled. We have recently summarized (*9*) various physical parameters of these two compounds, where references to earlier work can also be found. As previously shown these β forms can be pulled in large single crystals and are quite stable at room temperature, remaining unchanged after more than 6 years storage.

At elevated temperatures, the β to α transition becomes significant. Single crystals of β-$Gd_2(MoO_4)_3$ transform completely to the α form in 3 days at 800°C but only imperceptibly slowly at 600°C. Finely powdered β-$Gd_2(MoO_4)_3$ transforms completely in less than 3 days even at 400°C. Much more stability is observed in β-$Tb_2(MoO_4)_3$, which does not transform completely in the finely powdered state even after 7 days at 600°C. In addition to this better stability, β-$Tb_2(MoO_4)_3$ (which is also sometimes referred to as β-TMO, and β-$Gd_2(MoO_4)_3$ as β-GMO) is also easier to prepare in large uniform strain-free crystals, not showing the cracking and related growth problems of β-$Gd_2(MoO_4)_3$ (*10*).

Czochralski pulling to yield crystals of β-$Tb_2(MoO_4)_3$ is readily performed from a precious metal crucible in air, with a melt at about 1200°C. Presintered nominally stoichiometric powder prepared from $Tb_4O_7 + 6\ MoO_3$ was used as the feed material. Self-seeding of a single crystal occurred readily on a platinum wire with rotation at 100 rpm and a pulling rate of $\frac{1}{2}$ in. hr. The growth axis was found to be 110, the c axis being perpendicular to the growth direction. Growth on this as a seed yielded crystals up to $\frac{3}{4}$ in. diameter and several inches in length.

The X-ray diffraction pattern of as-grown β-$Tb_2(MoO_4)_3$, like β-$Gd_2(MoO_4)_3$, is made very complex by twinning (*9*). In both compounds (*9*, *11*) the application of pressure along [010] has been shown to interchange the a and b axes; this or an electric field application completely removes the twinning since the ferroelectricity and ferroelasticity are fully coupled. Since this coupling has been shown to be structural, all L-type materials are, therefore, expected to show this phenomenon below T_c. Structural (*4*) and other parameters (*9*) have been given. The transmission spectra of $Tb_2(MoO_4)_3$ are shown in Fig. 3; that of $Gd_2(MoO_4)_3$ was given previously (*1*).

Although not previously observed by us or others, we can now report high-temperature phase transitions in the L type molybdates of Eu, Gd, Tb, and Dy. This transition does not show up well, or not at all, on heating, but gives sharp DTA peaks on cooling with the usual supercooling (usually about 100°C); transition temperatures are, therefore, only approximate (estimated error up to ±30°C). The composite DTA curve of Fig. 4 illustrates the appearance and disappearance of the α, β, and γ forms of $Tb_2(MoO_4)_3$ with temperature cycling at heating and cooling rates of 20°C/min. The melting peak occurs at 1155°C whether the β or γ form is being melted, but the peak sizes are different as can

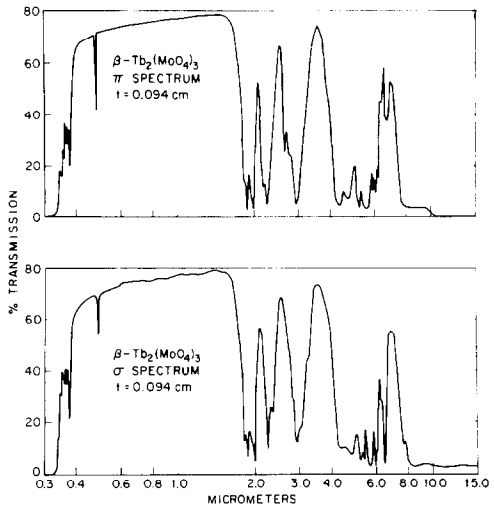

FIG. 3. Polarized absorption spectra for β-$Tb_2(MoO_4)_3$.

be seen in Fig. 4. By calibration with $SrCO_3$ (31.8 cal/g) the following approximate latent heats were established (with an estimated accuracy of ±15%). Melting of β-$Tb_2(MoO_4)_3$ at 1155°C $\Delta H_{1155} = 100$ kcal/mole; melting of γ-$Tb_2(MoO_4)_3$ at 1155°C $\Delta H_{1155} = 50$ kcal/mole; difference = transition β-$Tb_2(MoO_4)_3$ to γ-$Tb_2(MoO_4)_3$ $\Delta H_{1155} = 50$ kcal/mole.

Additional confirmation of this unusual $\beta \rightarrow \gamma$ transition was obtained from the high-temperature diffraction experiments shown in Fig. 5. This is a set of diffractometer traces between $2\theta = 25°$ and $2\theta = 32°$ taken at 2° 2θ/min on a G.E. XRD3

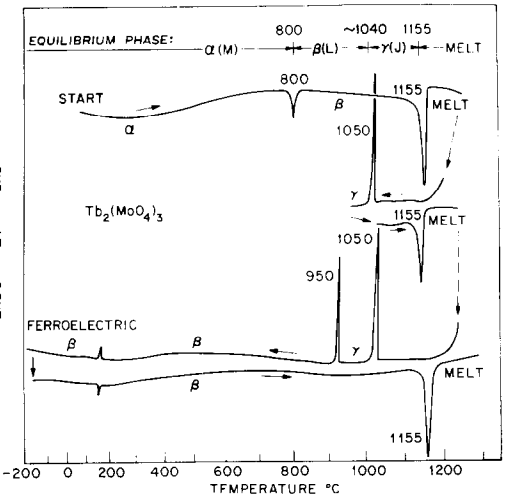

FIG. 4. Composite differential thermal analysis curve for $Tb_2(MoO_4)_3$. Heating and cooling rate 20°C/min in air.

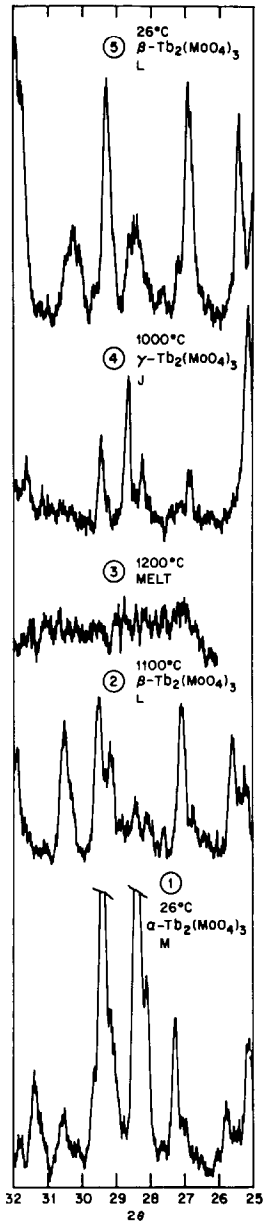

FIG. 5. Diffractometer traces of $Tb_2(MoO_4)_3$ taken with Cu$K\alpha$ radiation at 2° 2θ/min at the temperatures indicated.

machine equipped with a high-intensity Cu tube and an MRC high-temperature attachment. The sample was mounted on a vertical 5-mil platinum foil with a Pt–Pt–10% Rh thermocouple spot-welded to its back center. The temperatures were not completely uniform over the whole sample, varied somewhat during the experiment, and the values given are only approximate. Nevertheless the γ phase was not observed before melting but only after subsequent solidification. The β phase was the final product as expected, with some changes in the diffraction pattern due to orientation effects from solidification in a thin film and slight displacement of the foil sample holder. The d spacings and intensities of γ-$Tb_2(MoO_4)_3$ taken from the diffractometer trace are given in Table II. The indexing given is for a cubic structure with $a = 10.44$ Å. This is close to the average of the β-phase parameters 10.34, 10.39, and 10.65 Å. The extra line at 3.10 Å can be identified with the strongest line of Tb_4O_7. In view of the various uncertainties, the accuracy of the d values is estimated to be about $\pm 1\%$ and in view of this, refinement did not seem justified.

The γ to β transition for $Tb_2(MoO_4)_3$ and $Dy_2(MoO_4)_3$ is exothermic on cooling as expected, but for $Eu_2(MoO_4)_3$ and $Gd_2(MoO_4)_3$ it is endothermic on cooling. This could arise, for example, from exothermic heat emission being over-compensated by heat absorption originating in the supercooling temperature interval from a specific-heat difference between the β and γ phases, when the latter is smaller. This change may also indicate an additional change of structure within the Y field between Gd and Tb molybdate. Rapid quenching from the melt into liquid nitrogen or room-temperature mercury gave only the β phase for the Eu, Gd, and Tb compounds; the Dy to Y compounds gave the hydrates of structure K (*1*), which only appear to form with C structure compound.

TABLE II

X-RAY POWDER DATA FOR γ-$Tb_2(MoO_4)_3$ AT 1000°C[a]

hkl	d_{calcd} (Å)	d_{obsd} (Å)	I_{obsd}
2 0 0	5.22	5.28	vw
2 1 0	4.72	4.91	w
2 1 1	4.26	4.25	vs
2 2 0	3.69	3.69	vw
3 0 0, 2 2 1	3.48	3.52	s
3 1 0	3.30	3.30	vw
3 1 1	3.15	3.15	vw
—	—	3.10	m
2 2 2	3.01	3.02	w
3 2 1	2.79	2.82	vw
4 0 0	2.61	2.61	vs
4 2 0	2.33	2.31	vs
3 3 2	2.23	2.24	vw
4 2 2	2.13	2.15	vw
5 0 0, 4 3 0	2.09	2.09	vw
5 1 1, 3 3 3	2.01	2.01	m

[a] Indexing is for cubic, $a = 10.44$ Å.

Since the β-phase molybdates can be obtained as single crystal by pulling from the melt from Pr to Tb, including the γ region, the change γ to β is a relatively minor, nondestructive one. Accordingly, the γ structures must be closely related to the β structure.

Drobyshev *et al.* (*12*) have reported five forms of $Gd_2(MoO_4)_3$, namely L_1, L_2, N, N_5, and N_6. The DTA curves shown in this work are so diffuse that completeness of reaction or lack of stoichiometry must be suspected. In addition the material was prepared in the β form, cooled and then heated for DTA and powder X-ray diffraction. In such a cycle a metastable material may pass through other metastable forms (Ostwald's step rule or law of successive transformations) and so the significance of these results is questionable. In the case of $Pr_2(MoO_4)_3$ Drobyshev et al. (*13*) claim eight phases, designated N, N_1, N_2, N_3, N_4, BD, LD, and GD, but not L. The spacings of the diffraction lines for the five N forms in this system is essentially invariant. The only differences are in some of the intensities, which could have many causes. These results are incompatible with ours.

D. Mixed Molybdate–Tungstate Systems

A detailed study of the $Nd_2(MoO_4)_3$–$Nd_2(WO_4)_3$ system was presented previously (*2*). We have now completed five more pseudo-binary systems, those of lanthanum, samarium, gadolinium, holmium, and indium. These are shown in Figs. 6 through 10 and cover various types of end-member structural combinations. In the case of the gadolinium system of Fig. 8A, an actual equilibrium phase-diagram structure is shown, this being consistent with the phase rule and with the experimental DTA, quenching, and X-ray diffraction data. The phase relationships among the various forms of $Gd_2(MoO_4)_3$ have been discussed in the previous section. Only the experimental data are presented for the other four systems. The accuracy of the melting and transition temperatures is estimated to be ± 10 and ± 15°C, respectively, except when dashed lines indicate a greater uncertainty.

The indium system of Fig. 10, although not containing rare earths, is given as one showing no phase transitions. The unit cell parameters were determined from diffractometer traces; error bars are indicated in the figure. A maximum occurs in the unit cell volume, reflecting mainly the variation of the *b* parameter.

Figure 11 shows projections of the true monoclinic cells (*3*), orthorhombic subcells (*14*), and

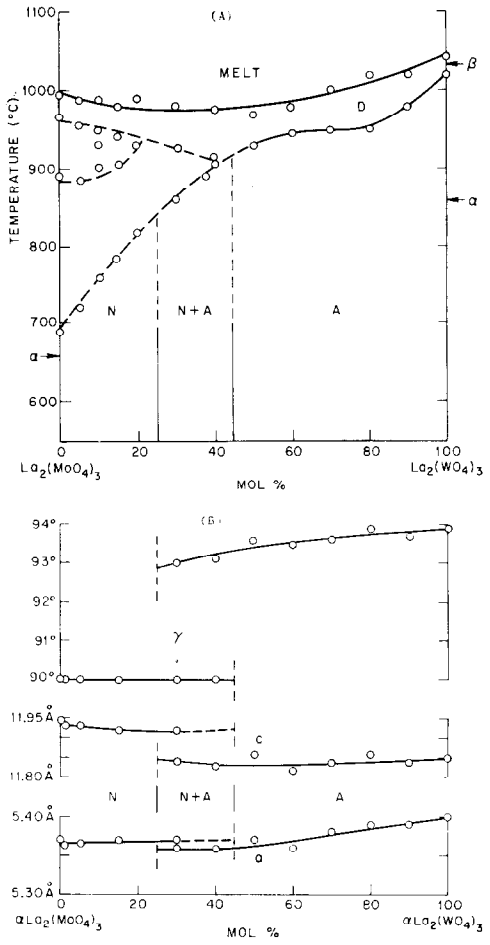

FIG. 6. Phase diagram (A) and lattice parameters for the scheelite-type subcell (B) for the $La_2(MoO_4)_3$–$La_2(WO_4)_3$ system.

tetragonal or distorted tetragonal scheelite-type subcells of α-neodymium molybdate (N) and tungstate (A) (*2*). The projections are viewed down the monoclinic *b*, orthorhombic *b*, and tetragonal *c* axes, these being identical ($b_m \equiv b_o \equiv c$). The other relationships between the orthorhombic and tetragonal subcells are

$$a = \tfrac{1}{2}\sqrt{a_0^2 + c_0^2/9}, \quad \gamma = 2\sin^{-1}(a_0/2a).$$

Although the true monoclinic cells are quite distinct, the family relationship can be most clearly seen in the scheelite-type tetragonal (or distorted tetragonal) subcells. The variation of the angle γ across the mixed neodymium molybdate tungstate system is shown in Fig. 11; the *a* and *c* variations are similar but less pronounced (*2*). Apart from the deviation of γ from the ideal value of 90° for the tetragonal N subcell, the other variation is in the

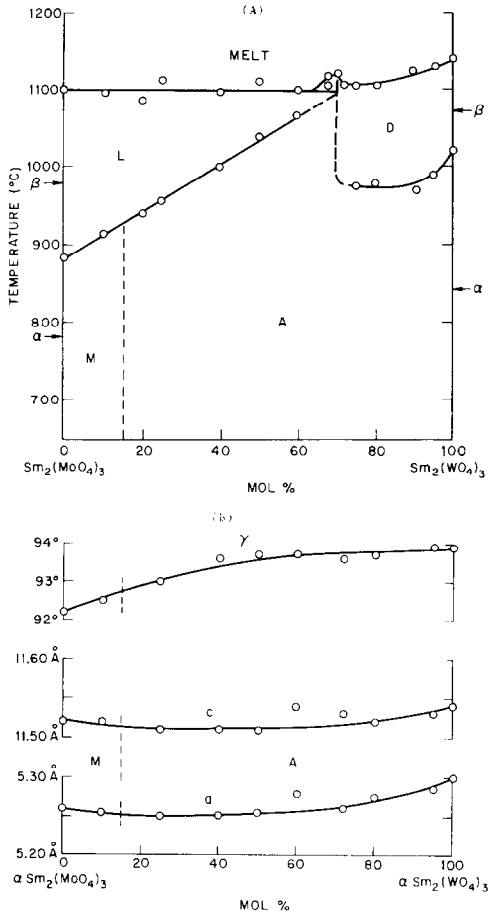

FIG. 7. Phase diagram (A) and lattice parameters for the scheelite-type subcell (B) for the $Sm_2(MoO_4)_3$–$Sm_2(WO_4)_3$ system.

manner of replacement of two Nd^{3+} and one vacancy for every three Ca^{2+} of the scheelite subcell. In the A structure this occurs in a highly ordered two full and one empty layer arrangement, and in the N structure (*3*) in the lower order arrangement shown; the barred circles here signify partial occupancy.

Although the study of single crystals is necessary for the establishment of the true cell parameters and the nature of the ordering, significant partial insight can be obtained from the tetragonal or pseudo-tetragonal scheelite-type subcell parameters shown in Figs. 6B to 9B. These were computed from the orthorhombic subcell parameters determined from the 220, 026, and 040 orthorhombic reflections which could in every case be located on the diffractometer traces. It is of course necessary to keep in mind that this is an abstracting process, the rigorousness of which can be established only when single-crystal data is available.

Another problem is the question of equilibrium. Reproducibility was difficult to attain in some of these systems, but we have found that 14 to 30 days sintering at 700°C with repeated grinding gives reproducible data; oxides rather than end-members were used in the case of low-temperature sintering to help attain equilibrium. We cannot be certain that the existence of a wide two-phase region, as in the holmium system, is an equilibrium relationship due to a mixture of end-members having a lower energy than a single continuously varying phase. Since a continuously varying phase does seem to occur in a system such as the neodymium one, the achievement of equilibrium does seem probable.

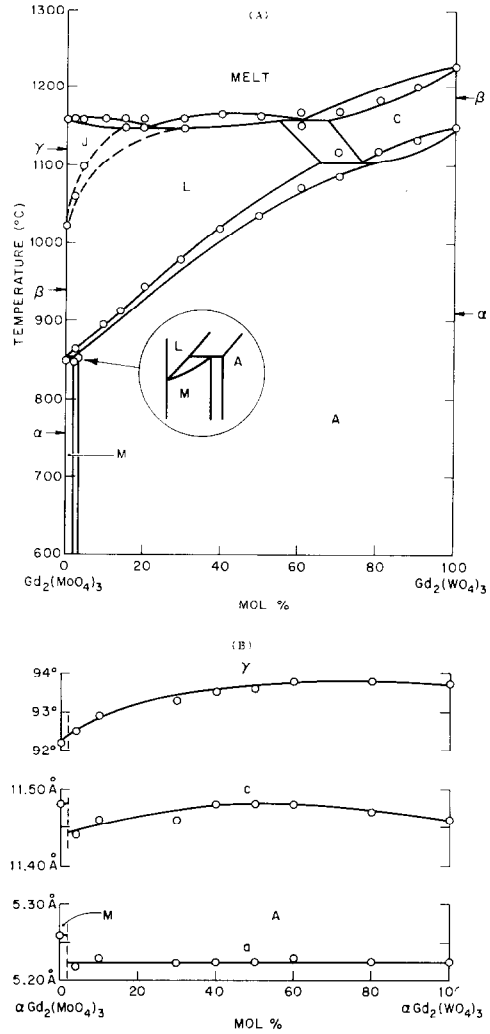

FIG. 8. Phase diagram (A) and lattice parameters for the scheelite-type subcell (B) for the $Gd_2(MoO_4)_3$–$Gd_2(WO_4)_3$ system.

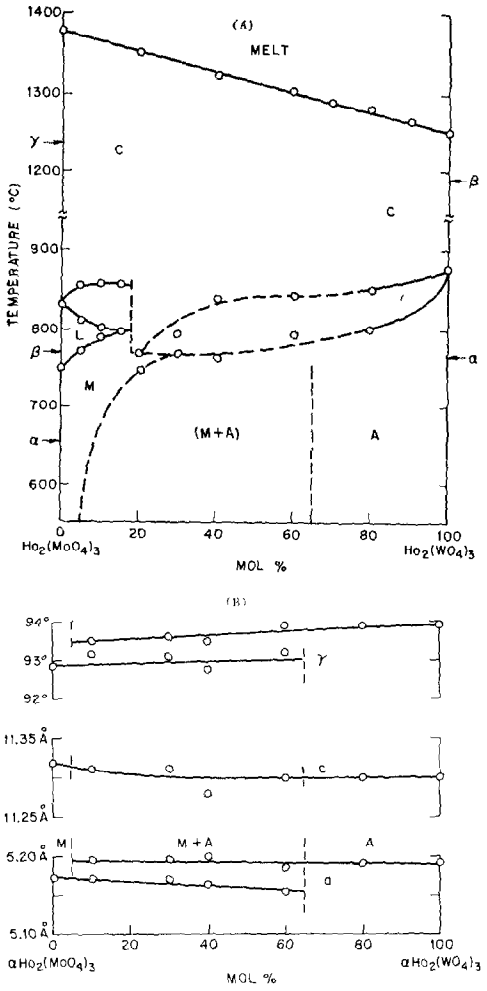

FIG. 9. Phase diagram (A) and lattice parameters for the scheelite-type subcell (B) for the $Ho_2(MoO_4)_3$–$Ho_2(WO_4)_3$ system.

The two N–A systems are quite different. In the neodymium system (Fig. 11) the N field is very narrow, extending only to about 2.5 mole%, and there is no evidence for a significant two phase region. In the lanthanum case of Fig. 6 the N field is much wider and the N and A structures appear to coexist, although as previously stated the possibility of nonequilibrium cannot be entirely ruled out.

In the three M–A systems a similarly wide range of behavior is observed. In the gadolinium system (Fig. 8) the M field is about 4 mole% wide and there is no evidence for a significant two phase region; here the subcell angle γ is continuous, but a and c are not. The holmium system (Fig. 9) shows an extensive region in which M and A appear to coexist;

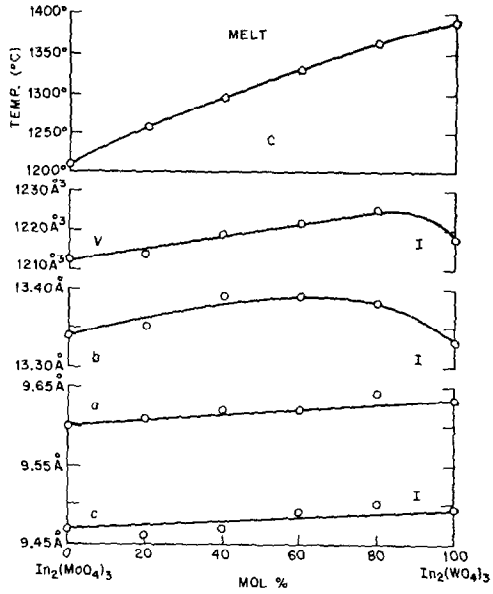

FIG. 10. Phase diagram and lattice parameters for the $In_2(MoO_4)_3$–$In_2(WO_4)_3$ system.

here c is continuous but a and γ are not. In the third M–A system, that of samarium (Fig. 7), the subcell parameters show no discontinuity at all. Nevertheless, examination of the sequence of Guinier

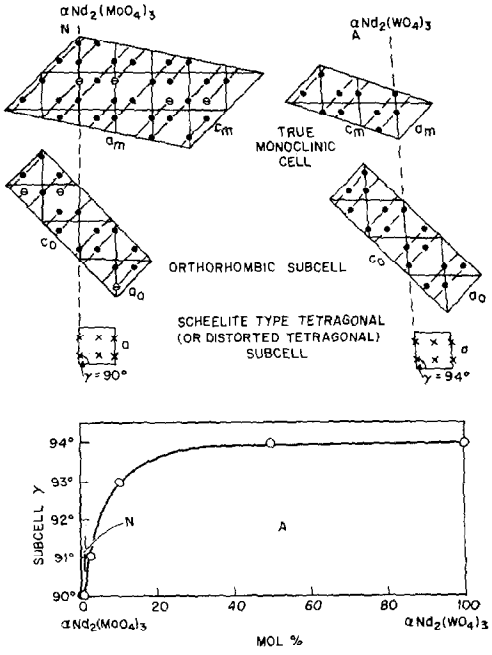

FIG. 11. Structures and subcell angle γ variation in the α-$Nd_2(MoO_4)_3$–$Nd_2(WO_4)_3$ system.

powder diffraction patterns shows a sequence of changes. The major change appears to occur near 15 mole% tungstate, and this is the position at which the M to A boundary is shown in Fig. 7. Confirmation of this was obtained from the powder second harmonic generation test as described by Kurtz and Perry (*15*). This showed the absence of a center of symmetry in $Sm_2(MoO_4)_3$, but its presence in the 20 to 100% $Sm_2(WO_4)_3$ compositions. There are nevertheless further changes, particularly between 25 and 60 mole%, consisting of the splitting and recombination of lines in the diffraction patterns. These are presumably indicative of slight changes in the order–disorder arrangement or small deviations from symmetry. All of the changes occur within the apparently uneventful subcell variation of Fig. 7B.

E. Discussion

From the details of the previous section and from our previous work (*2*), it can be concluded that there is a close relationship among the structures A, N*, M*, and D. There are nevertheless variations within the structures, and, e.g., it would not have been possible to assign α-$Sm_2(MoO_4)_3$ and α-$Ho_2(MoO_4)_3$ to the same structure type without observing the continuous change when the series of powder diffraction photographs of the molybdates of Sm, Eu, Gd, Tb, Dy, and Ho is assembled. We accordingly have assigned an asterisk to M* to indicate these variations. There are also variations in N*.

On this basis we recognize the overall relationship between A, N*, M*, and D by speaking of the A family of structures. This family comprises the low temperature forms of the larger ionic radius lanthanide tungstates and molybdates and is based on a scheelite type subcell with variable disorder in the way 2 Ln^{3+} ions replace 3 Ca^{2+} ions. There is eightfold oxygen coordination about the lanthanide ions in the two structures that have been fully determined in this family, α-$Eu_2(WO_4)_3$ (A) and α-$Nd_2(MoO_4)_3$ (N), and presumably also in the other member of this structure, all of which show scheelite or pseudoscheelite subcells. The membership of the various families and structures is summarized in Table III. The relationship between the L and J structures in the L family (Table III) is indicated by the nondestructive nature of the J to L transformation in single crystals grown from the melt. This family occurs for the intermediate radii tungstates and molybdates at intermediate temperatures as shown in Figs. 1 and 2. The oxygen coordination about Gd in β-$Gd_2(MoO_4)_3$ (L) is 7 (*4*). There is a tetragonal subcell, which is however not related to the scheelite structure.

TABLE III

STRUCTURE TYPES OF $Ln_2(WO_4)_3$ AND $Ln_2(MoO_4)_3$

Structure	Occurrence	Archetype and space group	Subcell	Refs.
A Family Structures (Ln 8-coordinated[a])				
A	α form of La to Y tungstates	α-$Eu_2(WO_4)_3$ *C*2/*c*	Scheelite type, $\gamma = 90°$	(1, 2, 7, 14)
D	β form of La to Eu tungstates	—	Pseudoscheelite, $\gamma \neq 90°$	(1)
M*[b]	α form of Sm to Ho molybdates	—	Pseudoscheelite, $\gamma \neq 90°$	(1)
N*	α form of La and Pr to Pm molybdates	α-$Nd_2(MoO_4)_3$ *C*2	Pseudoscheelite, $\gamma \neq 90°$	(2, 3, 7)
L Family Structures (Ln 7-coordinated[a])				
L	β form of Pr to Ho molybdates and α-Y molybdate	β-$Gd_2(MoO_4)_3$ $P42_1/m$[c]	Tetragonal	(1, 4, 9–11)
J*	γ form of Eu to Dy molybdates	γ-$Tb_2(MoO_4)_3$ (cubic[d])	—	—
C Family Structures (Ln 6-coordinated[a])				
C*	Molybdates: Er to Lu, Sc, In, Fe, Cr, Al	α-$Sc_2(WO_4)_3$ *Pnca*	—	(1, 5, 6)
	β-Y, γ-Ho, δ-Dy. Tungstates: Er to	$Fe_2(MoO_4)_3$ $P2_1/a$	*Pnca*	(16, 17)
	Lu, In, Sc, Al; β-form of Gd to Eu	$Tb_2(MoO_4)_3$ —	*Pnca*	(18)

[a] Where known.
[b] There is or may be some variation within the *structures (see text).
[c] Above T_c: below T_c it is *Pba*2.
[d] Cubic or close to cubic; *Pm*3*m* or subgroup.

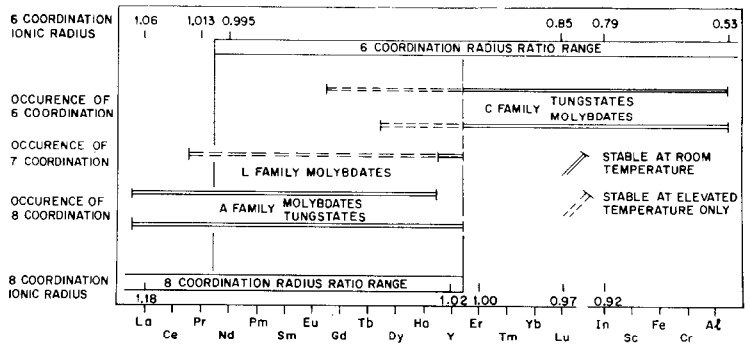

FIG. 12. Occurrence of the A, C, and L families shown against ionic size of the trivalent component.

In the C family there is 6-coordination about the trivalent lanthanide or transition metal ion. It has been reported (*16*, *17*) that $In_2(MoO_4)_3$ and $Fe_2(MoO_4)_3$, although having a C* structure (*Pnca*) subcell, are in fact monoclinic $P2_1/a$, with $a = 15.5$, $b = 9.2$, $c = 18.1$ Å and $\beta = 125°$ for the iron and $a = 16.34$, $b = 9.55$, $c = 18.76$ Å and $\beta = 125°$ for the indium compound. A brief examination (*18*) of a $Tm_2(MoO_4)_3$ crystal protected from reaction with atmospheric moisture showed a subcell identical with the $Sc_2(WO_4)_3$ structure, but indicated doubling of the c axis with $a = 10.00$, $b = 13.65$, and $c = 19.50$ Å. Rode *et al.* (*6*) have designated the lanthanide molybdates of this type C′, based on slight differences in the X-ray powder-diffraction pattern from that of $Sc_2(WO_4)_3$. This type of variation within C* is quite consistent with the structure family concept as proposed.

In Fig. 12, the occurrence of the 6-, 7-, and 8-coordinated families of structures are shown against the ionic radii of the trivalent ions. The radius ratio limits are based on a value of 0.732 with oxygen 1.38 Å. The radii used are taken from the recent compilation of Shannon and Prewitt (*19*). This set of radii, as well as others, places Y between Ho and Er; this position is confirmed for the molybdates and tungstates by the data of Figs. 1 and 2. The agreement observed in Fig. 12 must be considered to be better than one should expect, since these compounds clearly have an appreciable extent of covalent character.

The surprising diversity of structure types in these two series of compounds is systematized with the assignment of the eight or more structures into three families. We believe that the structures discussed here are equilibrium phases. Single-crystal studies, particularly of D, N*, J, and additional C* compounds, will be needed to obtain yet further insight into the relationships within and among these families of compounds.

Acknowledgments

We wish to thank J. L. Bernstein and D. L. Nitti for assistance with some of the diffraction work and S. C. Abrahams for helpful discussions.

References

1. K. NASSAU, H. J. LEVINSTEIN, AND G. M. LOIACONO, *J. Phys. Chem. Solids* **26**, 1805 (1965).
2. K. NASSAU, P. B. JAMIESON, AND J. W. SHIEVER, *J. Phys. Chem. Solids* **30**, 1225 (1969).
3. P. B. JAMIESON, S. C. ABRAHAMS, AND J. L. BERNSTEIN, *J. Chem. Phys.* **50**, 86 (1969).
4. E. T. KEVE, S. C. ABRAHAMS, AND J. L. BERNSTEIN, *J. Chem. Phys.* in press.
5. S. C. ABRAHAMS AND J. L. BERNSTEIN, *J. Chem. Phys.* **45**, 2745 (1966).
6. E. Y. RODE, G. V. LYSANOVA, V. G. KUZNETSOV, AND L. Z. GOKHMAN, *Russ. J. Inorg. Chem.* **13**, 678 (1968).
7. F. WEIGEL AND V. SCHERER, *Radiochim. Acta* **13**, 6 (1970).
8. V. E. PLYUSCHEV AND V. M. AMOSOV, *Dokl. Akad. Nauk. SSSR* **157**, 131 (1964).
9. E. T. KEVE, S. C. ABRAHAMS, K. NASSAU, AND A. M. GLASS, *Solid State Commun.* **8**, 1517 (1970).
10. H. J. BORCHARDT AND P. E. BIERSTED, *J. Appl. Phys.* **38**, 2057 (1967).
11. K. AIZU, A. KUMADA, H. YUMOTO, AND S. ASHIDA, *J. Phys. Soc. Jap.* **27**, 511 (1969).
12. L. A. DROBYSHEV, I. T. FROLKINA, V. I. PONOMOREV, Y. Y. TOMASHPOLSKII, Y. N. VENEVTSEV, AND G. S. ZHDANOV, *Sov. Phys. Crystallogr.* **15**, 53 (1970).
13. L. A. DROBYSHEV, V. I. PONOMAREV, I. T. FROLKINA, AND N. V. BELOV, *Sov. Phys. Crystallogr.* **15**, 391 (1970).
14. D. H. TEMPLETON AND A. ZALKIN, *Acta Crystallogr.* **16**, 762 (1963).
15. S. K. KURTZ AND T. T. PERRY, *J. Appl. Phys.* **39**, 3798 (1968).
16. L. M. PLYASOVA, R. F. KLEVTSOVA, S. V. BORISOV, AND L. M. KEFELI, *Sov. Phys. Crystallogr.* **13**, 29 (1968).
17. L. M. PLYASOVA, R. F. KLEVTSOVA, S. V. BORISOV, AND L. M. KEFELI, *Sov. Phys.-Dokl.* **11**, 189 (1966).
18. J. L. BERNSTEIN AND K. NASSAU, unpublished data.
19. R. D. SHANNON AND C. T. PREWITT, *Acta Crystallogr. Sect. B.* **25**, 925 (1969).